

EXPERIMENTAL AND COMPUTATIONAL INVESTIGATION FOR 3-D DUCT FLOW WITH MODIFIED ARRANGEMENT RIBS TURBULATORS

by

Khudheyer MUSHATET* and Sarah NASHEE

Mechanical Engineering Department, College of Engineering,
Thi-Qar University, Nassiriya

Original scientific paper
<https://doi.org/10.2298/TSCI190813093M>

A combined numerical and experimental study is conducted to test the heat transfer enhancement and friction factor characteristics for a rectangular duct fitted with three cases of ribs turbulators: continuous ribs, intermittent-continuous-intermittent ribs, and intermittent ribs. Experiments are conducted within a turbulent flow for Reynolds numbers values varied from 10000 to 35000, pitch ratio equal to 5 and height ratio of 0.33. The numerical study carried out using ANSYS FLUENT17.2. The turbulence is modeled by using k-ε model. The results showed that the case of intermittent ribs provide the highest over performance factor while the continuous ribs indicate less overall performance factor among the considered cases. In addition, the results show that the highest values of the friction factor are marked from the case of intermittent ribs and then the case of intermittent-continuous-intermittent ribs followed by continuous rib case. The continuous rib case showed the lowest friction factor. The experimental results showed a good agreement with the computational results.

Key words: ribs turbulators, turbulent flow, overall performance

Introduction

Different cooling methods have been developed over the previous years to ensure that many thermal applications maintain a level consists of maximum internal heat transfer. The obstacles are used to enhance the heat transfer process in various cooling passages, e.g., gas turbine blades, heat exchangers, guide vanes, radiators of s vehicles and combustor walls, Wang and Sunden [1]. Han and Zhang [2] conducted experiments to test heat transfer and friction factor characteristics of a roughened square channel with various angled and V-shaped broken ribs. The attack angle of ribs was 45° and 60°. Reynolds number was ranged from 15000-90000. It was found that broken ribs gave a heat transfer enhancement of 2.5-4 as level while the continuous ribs (CR) was from 2-3. Liou and Hwang [3, 4] presented intensive investigations to examine the thermal performance of square, triangular and semi-circular ribs by employing laser holographic interferometry. They reported that the square ribs gave the best performance among those of ribs tested. Tanda [5] conducted an experimental study to test the heat transfer enhancement for a rectangular channel with one wall ribbed. The aspect ratio was 5:1 with CR and 90° broken ribs. The results confirmed that the enhancement in heat transfer for 90° broken ribs was around 1.8 times than the CR. Also by experimental

* Corresponding author, e-mail: khudheyersalim@gmail.com

study, Sahu and Bhagoria [6] examined the effect of 90° broken ribs attached to a heated absorber plate. The Reynolds number range was from 3000-12000. The aspect ratio of the rectangular channel had a fixed value at 8 with height to hydraulic diameter ratio (e/D_h) of 0.0338 and roughness height e of 1.5 mm. In addition, the experiments used a range of roughness and pitch varied from 10-30. As a result of these investigations, they observed that there was a high increase in Nusselt number value at low Reynolds number. The heat transfer coefficient was at a maximum value at a pitch of 2 cm. Moreover, the experimental results showed that the Nusselt number increased about 1.25-1.4 times that of the smooth channel. Furthermore, Wang and Sunden [7] conducted a series of experiments on the turbulent heat transfer and friction factor in a square duct roughened by consistent and intermitted ribs on one surface. For both cases, the rib e/D_h ratio was 0.15. The rib pitch ratio was 12. The experimental results of this work gave reported that the heat transfer coefficient was strongly influenced by the shape of the ribs. Keshmiri *et al.* [8] tested the heat transfer and enhancement by using a rectangular channel for three amount of pitch ratio, p/e , 6, 9, and 12. The results presented a reported that the ratio $p/e = 9$ gave the greatest heat transfer value and the pressure loss obtained its maximum for this p/e ratio. Another experimental study was done by Rallabandi *et al.* [9] to evaluate heat transfer enhancement in a square duct roughened by 45° ribs on two opposite walls. The experimental work used blockage ratio, e/D_h , changed from 0.1-0.18 and p/e ranged from 5-10. The results of the experimental work showed that a larger value of e/D_h and a smaller value of p/e gave the maximum value of heat transfer coefficient. Mushatet *et al.* [10] performed a numerical investigation test the heat transfer through an obstacle sudden expansion channel. Rectangular obstacles mounted behind the expansion region on the upper and lower surface of the channel employed. Three amount of expansion ratio equal to 1.5, 1.75, and 2 were applied. It was found that the heat transfer enhanced more as the obstacles thickness increases. Skullong *et al.* [11] studied heat transfer features in a square duct fitted with different rib heights for the turbulent flow, Reynolds number ranged from 4000-40000. The results verified that the usage of ribs showed considerable heat transfer augmentation where Nusselt number increased with the increase of Reynolds number value. Also, Eren *et al.* [12] performed experimental work about heat transfer improvement in a rectangular channel by using perforated ribs. Measurements were performed with a height ratio of 0.1 and by using affixed rib pitch ratio of $p/e = 12$. It was found that the roughed duct gave a value of heat transfer more about 34.1% compared to the smooth channel. Experimental and theoretical investigation were done by Smaism [13] for using rectangular duct with rectangular ribs of p/e from 6.66-15 and different heights. It was found that the increasing in the height of the ribs caused increase in heat transfer and thermal performance of the duct.

The present study tests heat transfer enhancement in a 3-D straight rectangular duct with rib turbulators. The ribs are placed on the lower surface of the duct which is heated with a fixed value of heat flux (1000 w/m²). The work of the ribbed duct includes three cases: CR, intermittent-continuous-intermittent ribs (ICIR), and intermittent ribs (IR). The Reynolds number is ranged from 10000-35000. The aim of the present study is to present modified ribs arrangement to enhance heat transfer in a heated duct. To the author's knowledge, there is no study documented on the considered ICIR arrangement.

Experimental Procedure and data reduction

An experimental set-up has been designed to study the effects of the rib turbulators on heat transfer and friction factor characteristics for various values of air-flow velocities corresponding for Reynolds numbers changed from 10000-35000. The schematic diagram of the

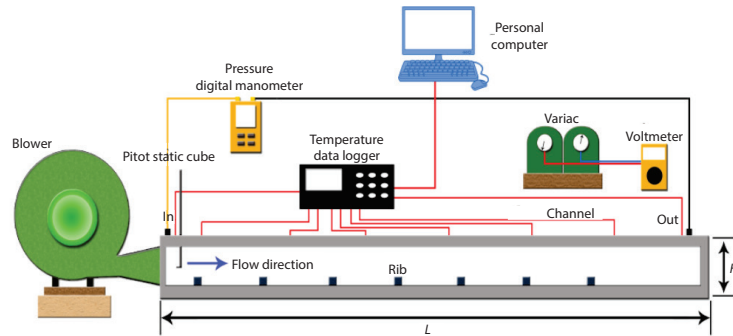


Figure 1. The experimental set-up

experimental set-up is display in fig. 1. The duct has a total length of 1 m, width equal to 15 cm, and height is 6 cm. It is manufactured by using 2 mm thickness of Galvanized iron and 2 mm thick plexiglas plates for the two sides. The duct is exposed to the heat flux on the bottom surface by a heater of constant heat flux by the ohmic method. The upper and side walls are not insulated. In theoretical analysis, the heat loss is accounted by conjugate heat transfer while in experimental analysis the dependence was on the matrix bottom wall temperature distribution besides to bulk temperature which is affected by the transfer of heat from the duct walls. The ribs made from Galvanized iron that have been connected to the wall by using glue. Three different cases of rib turbulators arrangement are supplied to achieve the best thermal performance. The $p/e = 5$ and $e/H = 0.33$. In addition there are three values of ribs lengths, $s = 30, 60, 150$ mm.

In the first case, seven CR are arranged on the hot surface of the duct, while the second case includes seven rows arranged sequentially as intermittent-continuous-intermittent and the third case, seven rows of IR are tested. These cases are shown in fig. 2. The air which a working fluid at ambient temperature is pushed from the laboratory room through a blower and the flow velocity is controlled by adjusting the frequency of the blower. The temperature of the bottom test surface is measured by 18 (*k*-type) thermocouple sensors distributed for six matrices, each matrix has three sensors. These sensors are connected to digital data logger to display the temperature values on computer screen. As for pressure difference, digital pressure manometer is employed to gain the values by two static pressure probe at the entrance and the outlet of the duct. Furthermore, at the entrance and the outlet of the duct, there are two *T*-type thermocouple sensors to report the values of the inlet and outlet temperature.

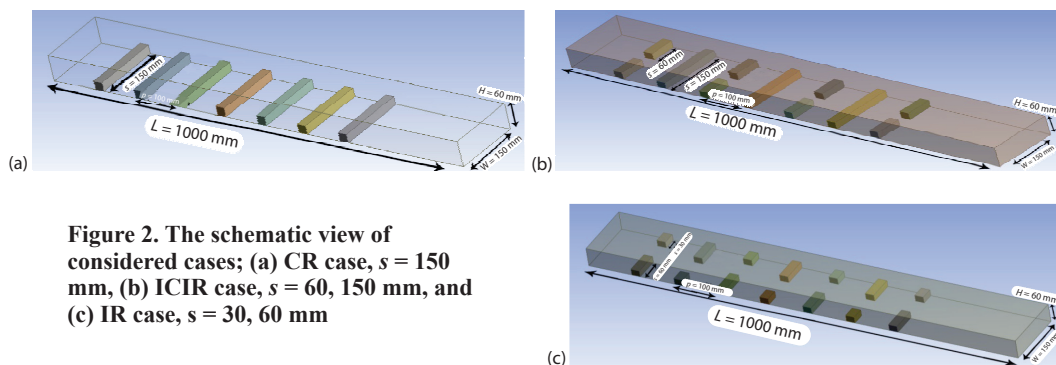


Figure 2. The schematic view of considered cases; (a) CR case, $s = 150$ mm, (b) ICIR case, $s = 60, 150$ mm, and (c) IR case, $s = 30, 60$ mm

The heat flux, Q , is obtained:

$$Q = VI \quad (1)$$

The mean heat transfer coefficient is calculated:

$$h = \frac{Q}{A_s} (T_w - T_b) \quad (2)$$

Where the mean wall temperature is calculated:

$$T_w = \sum_1^n \frac{T_{wi}}{n} \quad (3)$$

The mean bulk temperature is gained:

$$T_b = \frac{T_{out} + T_{in}}{2} \quad (4)$$

The average Nusselt number is introduced:

$$Nu_{avg} = \frac{hD_h}{k} \quad (5)$$

where h is the mean heat transfer coefficient.

The friction factor, can be defined by using Darcy Weisbach equation:

$$f = \frac{\Delta p D_h}{\frac{1}{2} \rho u_{avg}^2 L} \quad (6)$$

The overall performance factor, η , [14] is given:

$$\eta = \frac{Nu}{Nu_0} / \left(\frac{f}{f_0} \right)^{1/3} \quad (7)$$

Mathematical model

The hypothesis of this model is a 3-D incompressible turbulent flow, gravity effect is neglected. The continuity equation [14], momentum equation, and energy equation [15] in the fluid region can be expressed:

The continuity equation:

$$\frac{\partial u}{\partial x} + \frac{\partial v}{\partial y} + \frac{\partial w}{\partial z} = 0 \quad (8)$$

Momentum equation in x -direction:

$$\begin{aligned} \rho \left(\frac{\partial u^2}{\partial x} + \frac{\partial uv}{\partial y} + \frac{\partial uw}{\partial z} \right) = & -\frac{\partial P}{\partial x} + \frac{\partial}{\partial x} \left(2\mu_{eff} \frac{\partial u}{\partial x} \right) + \frac{\partial}{\partial y} \left(\mu_{eff} \frac{\partial u}{\partial y} \right) + \\ & + \frac{\partial}{\partial z} \left(\mu_{eff} \frac{\partial u}{\partial z} \right) + \frac{\partial}{\partial y} \left(\mu_{eff} \frac{\partial v}{\partial x} \right) + \frac{\partial}{\partial z} \left(\mu_{eff} \frac{\partial w}{\partial y} \right) \end{aligned} \quad (9)$$

Momentum equation in y-direction:

$$\rho \left(\frac{\partial vu}{\partial x} + \frac{\partial v^2}{\partial y} + \frac{\partial vw}{\partial z} \right) = -\frac{\partial P}{\partial y} + \frac{\partial}{\partial x} \left(\mu_{\text{eff}} \frac{\partial v}{\partial x} \right) + \frac{\partial}{\partial y} \left(2\mu_{\text{eff}} \frac{\partial v}{\partial y} \right) + \frac{\partial}{\partial z} \left(\mu_{\text{eff}} \frac{\partial v}{\partial z} \right) + \frac{\partial}{\partial x} \left(\mu_{\text{eff}} \frac{\partial u}{\partial y} \right) + \frac{\partial}{\partial z} \left(\mu_{\text{eff}} \frac{\partial w}{\partial y} \right) \quad (10)$$

Momentum equation in z-direction:

$$\rho \left(\frac{\partial wu}{\partial x} + \frac{\partial wv}{\partial y} + \frac{\partial w^2}{\partial z} \right) = -\frac{\partial P}{\partial z} + \frac{\partial}{\partial x} \left(\mu_{\text{eff}} \frac{\partial w}{\partial x} \right) + \frac{\partial}{\partial y} \left(2\mu_{\text{eff}} \frac{\partial w}{\partial y} \right) + \frac{\partial}{\partial z} \left(2\mu_{\text{eff}} \frac{\partial w}{\partial z} \right) + \frac{\partial}{\partial x} \left(\mu_{\text{eff}} \frac{\partial u}{\partial z} \right) + \frac{\partial}{\partial y} \left(\mu_{\text{eff}} \frac{\partial v}{\partial z} \right) \quad (11)$$

Energy equation:

$$\frac{\partial uT}{\partial x} + \frac{\partial vT}{\partial y} + \frac{\partial wT}{\partial z} = \frac{\partial}{\partial x} \left(\Gamma_{\text{eff}} \frac{\partial T}{\partial x} \right) + \frac{\partial}{\partial y} \left(\Gamma_{\text{eff}} \frac{\partial T}{\partial y} \right) + \frac{\partial}{\partial z} \left(\Gamma_{\text{eff}} \frac{\partial T}{\partial z} \right) \quad (12)$$

For energy dissipation rate, ε :

$$\Gamma_{\text{eff}} = \Gamma + \Gamma_t \quad (13)$$

where $\Gamma_t = \nu_t/\sigma_t$, σ_t is the turbulent Prandtl number.

The standard k - ε model which is one of the most widely utilized models is used to model the turbulence in the flow. It is a semi-empirical model with two equations: one is a transport equation for turbulent kinetic energy, k , and the other for dissipation of turbulent kinetic energy, ε .

For turbulent kinetic energy, k :

$$\rho \left[\frac{\partial}{\partial x} (ku) + \frac{\partial}{\partial y} (kv) \right] + \frac{\partial}{\partial z} (kw) = \frac{\partial}{\partial x} \left(\frac{\mu_t}{\sigma_k} \frac{\partial k}{\partial x} \right) + \frac{\partial}{\partial y} \left(\frac{\mu_t}{\sigma_k} \frac{\partial k}{\partial y} \right) + \frac{\partial}{\partial z} \left(\frac{\mu_t}{\sigma_k} \frac{\partial k}{\partial z} \right) + G - \rho\varepsilon \quad (14)$$

For energy dissipation rate, ε :

$$\rho \left[\frac{\partial}{\partial x} (\varepsilon u) + \frac{\partial}{\partial y} (\varepsilon v) + \frac{\partial}{\partial z} (\varepsilon z) \right] = \frac{\partial}{\partial x} \left(\frac{\mu_t}{\sigma_\varepsilon} \frac{\partial \varepsilon}{\partial x} \right) + \frac{\partial}{\partial y} \left(\frac{\mu_t}{\sigma_\varepsilon} \frac{\partial \varepsilon}{\partial y} \right) + \frac{\partial}{\partial z} \left(\frac{\mu_t}{\sigma_\varepsilon} \frac{\partial \varepsilon}{\partial z} \right) + C_{1\varepsilon} \rho \frac{\varepsilon}{k} G - C_{1\varepsilon} \rho \frac{\varepsilon}{k} \quad (15)$$

where G is referred to the generation term and is given:

$$G = \mu_t \left[2 \left(\frac{\partial u}{\partial x} \right)^2 + 2 \left(\frac{\partial v}{\partial y} \right)^2 + 2 \left(\frac{\partial w}{\partial z} \right)^2 + \left(\frac{\partial v}{\partial y} \frac{\partial u}{\partial x} \right)^2 + \left(\frac{\partial v}{\partial z} \frac{\partial w}{\partial x} \right)^2 + \left(\frac{\partial v}{\partial z} \frac{\partial w}{\partial y} \right)^2 \right] \quad (16)$$

To solve the equations, boundary conditions are to be imposed on the boundaries of the computational domain. At the Inlet, uniform inlet velocity (u 1.75-6.1 m/s) is imposed which is corresponding to Reynolds number range from 10000-35000 and the flow is isothermal ($T = T_{\text{in}} = 298$ K). At the walls and ribs, no-slip condition ($u = v = w = 0$) are obtained. In addition $\partial P/\partial n = 0$, $k = 0$ and $\varepsilon = 0$. At exit, the relative gage pressure is zero and smooth exit for the studied variables are imposed.

Numerical analysis

The commercial FLUANT 17.2 code is utilized to solve the 3-D mathematical model based on finite volume technique. The veracity and the reliability of the numerical results are secured by an accurate test of the grid-independence to estimate the most favorable mesh size.

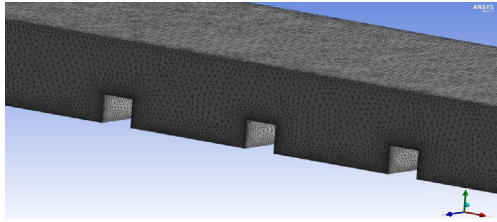


Figure 3. The considered mesh generation

The tetrahedral mesh is used as shown in fig. 3. It is clear that the mesh is very fine near the walls and around the ribs to capture the flow behavior in these areas. Table 1 shows a sample of the tested grids at $Re = 20000$. The fourth row of the table 1 for each ribs configuration is adopted in this study.

Table 1. Tested grids for the studied cases at $Re = 20000$

Case	Number of mesh elements	Nu	f
CR	2210733	92.0123	0.0563
	2344658	90.684	0.0571
	2412236	89.559	0.0576
	2549349	88.782	0.058
ICIR	2465253	91.66	0.078
	2486390	92.78	0.081
	2524667	93.34	0.084
	2579547	93.82	0.085
IR	2577377	100.832	0.113
	2627738	103.204	0.118
	2747589	101.98	0.114
	2810848	102.88	0.116

Results and discussion

The collected results are gained for rectangular ribs in a 3-D rectangular duct in turbulent flow regime. Three rib configurations (CR, ICIR, IR) are selected with ribs height ratio $e/H = 0.33$, the pitch ratio $p/e = 5$, and the Reynolds number is ranged from 10000-35000. The results are compared with plane duct to evaluate the thermal-hydrodynamics performance.

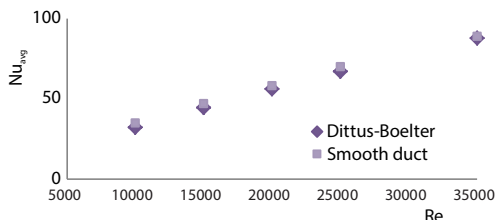


Figure 4. Comparison of the present results with the empirical correlations of Dittus-Boelter [16]

Prior to the experiments on the duct with rib turbulators, the Nusselt number and friction factor are calculated for the smooth rectangular duct in order to extend the reliability to the experimental work. The collected average Nusselt number is compared with the results obtained from the empirical equation of Dittus-Boelter [16] as shown in fig. 4. The comparison provides an acceptable agreement where the deviation between the results is not exceeding 4%:

$$Nu = 0.023 Re^{0.8} Pr^{0.4} \quad (17)$$

Also, the friction factor is measured and compared with the empirical Blasius equation [16] as shown in fig. 5. The relative deviation between the results is 6.8%:

$$f = 0.316 Re^{-0.25} \quad (18)$$

Figure 6 clarifies the influence of the cases of CR, ICIR, and IR on average Nusselt number. The experimental results of the case of IR gave the highest values for the Nusselt number followed by the case of ICIR, and then the CR case. That is because of the strength and size of re-circulating zones behind the ribs at the IR due to the increase in the edges compared to the other cases. These edges lead to increase the flow restriction creating strong vortices cause disturbing the boundary-layer and increase turbulence mixing of the flow field and thus enhancing heat transfer. As compared with smooth duct, all the cases that tested show enhancement in Nusselt number.

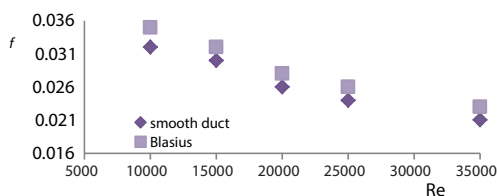


Figure 5. Comparison the result of present work with the correlation of Blasius [16] for friction factor

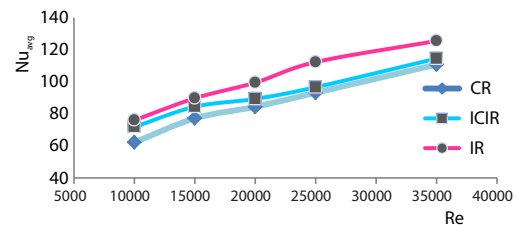


Figure 6. The variation of Nusselt number with Reynolds number for the considered cases

In the current work, all the pressure losses include losses due to friction and due to drag force exerted by ribs. It is found that the case of IR show the highest values for the friction, while the case of CR gives the lowest values of the friction factor. In addition, the variation of friction factor with Reynolds number for duct fitted with a different arrangement of rib tabulators. It is noticed that the increase in Reynolds number leads to a decrease in the friction factor. Figure 7 displays the comparison of the cases through a relation between the Reynolds number and friction factor.

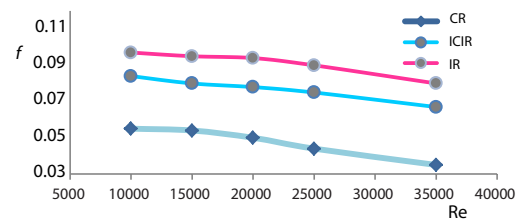


Figure 7. The variation of friction factor with Reynolds number for the considered cases

The mechanisms of heat transfer enhancement can be explained by the fact that the rib turbulators which cause the secondary flow can directly impinge to the duct surface. The boundary-layer becomes thinner and mixing between hot surface and cold fluid occurs. The experimental results of these tests showed an improvement in overall performance as compared to the smooth duct, especially at the case of IR that showed the highest performance of the three tested cases. This may be

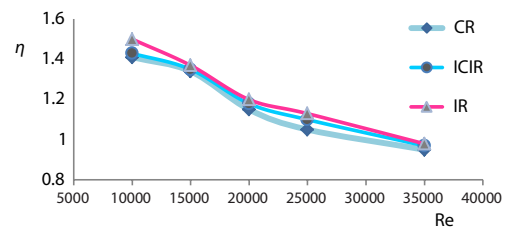


Figure 8. The influence of the ribs arrangements on the overall performance for the considered cases

due to better turbulence mixing which increases the contact of cold air with a hot duct surface, consequently enhancing heat transfer rates. Conversely, the CR showed the minimum values of the overall performance. Namely, the results of the experimental work reported that the case of IR gave the best performance, it is reached to 1.5 at $Re = 10000$, as in fig. 8

A comparison is made between the theoretical results and the results of the experimental work to obtain the credibility of the results are attained. A comparison is made between the results of Nusselt numbers as well as the results of the friction factor. The relative deviation between the results of the Nusselt number is not exceeded 7% while the relative deviation of the results of the friction factor is equal to 14%, as in figs. 9 and 10.

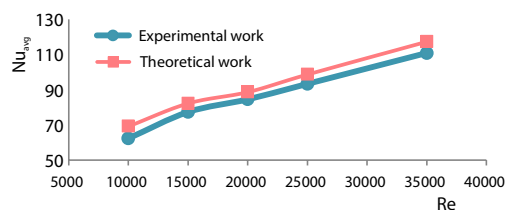


Figure 9. The comparison between Nu_{avg} of the experimental and numerical work for CR case

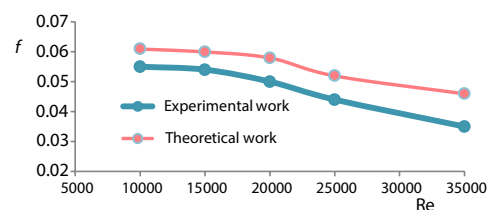


Figure 10. The comparison between experimental and numerical work for the CR case

Figure 11 clarifies a comparison between the experimental and theoretical results of the Nusselt number of the ICIR case. The results show a relative deviation of 6%, while the results of the friction coefficient values show a relative deviation of 6%, as in fig. 12.

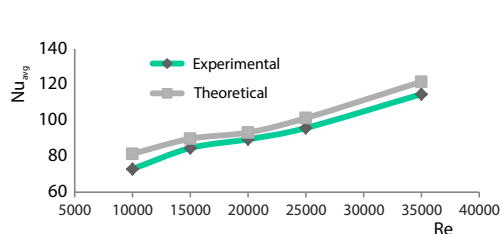


Figure 11. The comparison between the experimental and Nu_{avg} results for ICIR case

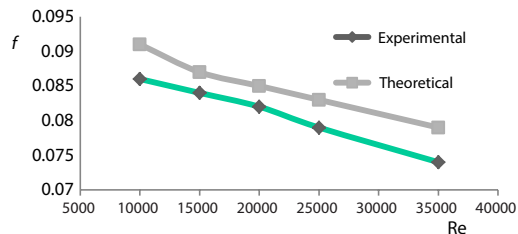


Figure 12. The comparison between the results of friction factor of the experimental and numerical work for ICIR case

For the case of IR, the results of the experimental and theoretical tests of Nusselt number and friction factor are compared. Figure 13 shows that the relative deviation does not exceed 6% for Nusselt number results. In addition, fig. 14 displays 8% deviation between the theoretical and experimental results of friction factor.

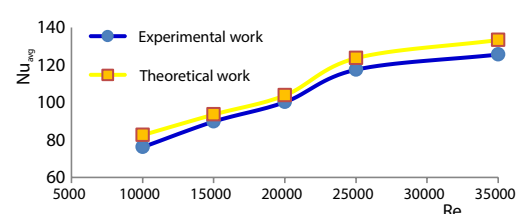


Figure 13. The comparison between the experimental and numerical Nusselt number results for IR case

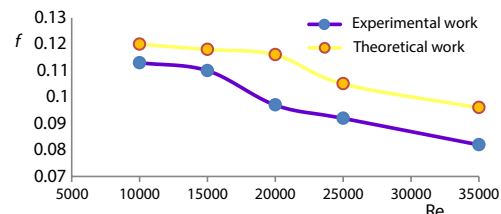


Figure 14. The comparison between the results of friction factor of the experimental and numerical work for IR case

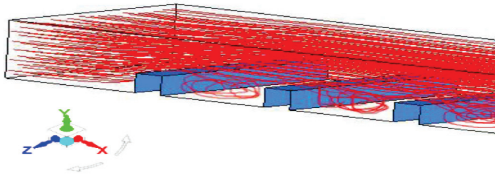


Figure 15. Streamlines for CR case at Re = 20000

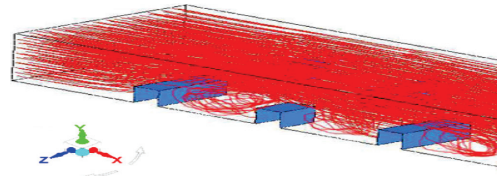


Figure 16. Streamlines for ICIR case at Re = 20000

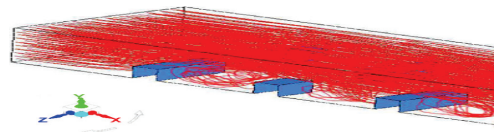


Figure 17. Streamlines for IR case at Re = 2000

The nature of the fluid-flow for all the entire ribbed duct domain is introduced in figs. 15-17 for all cases to track the path that followed by the fluid. All cases show separation flow after the regions of the ribs and the swirls form towards upstream which enhances the turbulence mixing of the flow field, to increase the heat transfer. These swirls are increased in IR case. It appears less in the case of ICIR and then decreases significantly in the case of CR.

Figures 18 and 19 show a comparison between the present results and published results of Gupta *et al.* [17]. They performed an intensive study to calculate the Nusselt number and friction factor for a square duct with CR arranged with $p/e = 10$ with $e/D_h = 0.06$ and tested for with and without a gap. The case without gap and a 90° of attack angle are selected to test. It can be observed that the relative deviations between the results not exceed 17% and 18% for Nusselt number and friction factor results, respectively. This deviation is due to a difference in the value of pitches ratio and the duct configuration.

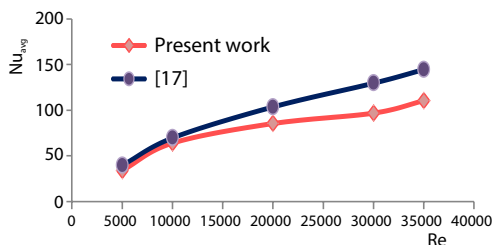


Figure 18. The comparison between the current study and [17] for Nusselt number results

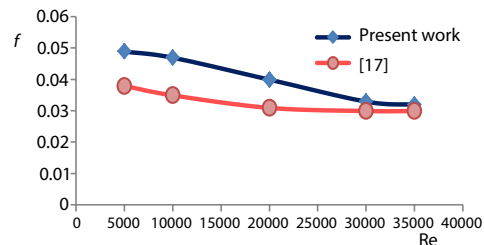


Figure 19. The comparison between the current study and [17] for friction factor results

Empirical correlations for collected experimental data have been conducted. The XL-STAT softer is adopted to get the form of this analysis. Two empirical correlations of the average Nusselt number and friction factor for the tested rib turbulators cases are proposed for $Re = 10 \cdot 10^3$ to $35 \cdot 10^3$. Correlation equations are calculate depending upon the obstruction ratios made by the rib turbulators, where represents the ratio between the area of obstruction the surface area of the duct, as shown in the equations below:

For the ribs rows in the odd position:

$$C_1 = \frac{A_r}{A_C} \quad (19)$$

For the ribs rows in the even position:

$$C_2 = \frac{A_{r2}}{A_C} \quad (20)$$

where $A_C = WH$, $A_{r1} = se$ (for the ribs rows in the odd position), $A_{r2} = se$ (for the ribs rows in the even position).

Equations (21) and (22) show an empirical equation of Nusselt number and friction factor for the duct with rib turbolators, respectively.

$$\text{Nu} = 1.1412C_1^{-0.448}C_2^{0.09392} \text{Pr}^{0.4} \text{Re}^{0.40727} \quad (21)$$

$$f = 0.1407C_1^{-1.7702}C_2^{0.54742} \text{Pr}^{0.4} \text{Re}^{-0.2267} \quad (22)$$

The maximum deviations between the predicted and experimental data are within 3% and 2% for Nusselt number and friction factor, respectively.

The uncertainty

In order to ensure the certainty of the results obtained from the experimental works, the three-time CR test was repeated under the same conditions to calculate Nusselt number and friction factor for all Reynolds number values. The deviation between the results of the three tests did not exceed 1.21% and 2.33% for Nusselt number and friction factor, respectively.

The mean, \bar{x}_{mean} :

$$\bar{x}_{\text{mean}} = x_{\text{avg}} = \frac{\sum_{i=1}^n x_i}{n} \quad (23)$$

where x_i is the values of each measurement and n – the total number of measurements of x .

The standard deviation of x denoted by σ :

$$\sigma = \sqrt{\frac{\sum_{i=1}^n (x_i - \bar{x})^2}{n-1}} \quad (24)$$

The standard deviation of the mean. It is also called the standard error is denoted by σ_m :

$$\sigma_m = \frac{\sigma}{\sqrt{n}} \quad (25)$$

Conclusions

The following conclusions can be obtained from this study.

- Nusselt numbers values significantly increases with the presence of ribs as compared with the values that gained from smooth duct.
- Nusselt number has the highest values in IR case and lowest values in CR case.
- The duct with intermitted ribs indicates the maximum value of the overall performance ($\eta = 150\%$) at $\text{Re} = 10000$.
- The friction factor values increase in IR case and have the lowest values in the CR case.

Nomenclature

A_s – surface area of the bottom wall, [m²]
 A_r – obstruction area of ribs row, [m²]

C_1 – obstruction ratio for the ribs rows in the odd position

C_2 – obstruction ratio for the ribs rows in the even position	T_{out} – outlet temperature, [K]
D_h – hydraulic diameter, [m]	T_w – wall temperature, [K]
e – rib height, [m]	u – average velocity in x -direction, [ms^{-1}]
f – friction factor	V – voltage, [V]
h – mean heat transfer coefficient, [$Wm^{-2}K^{-1}$]	v – average velocity in y -direction, [ms^{-1}]
H – height of duct, [m]	W – width of duct, [m]
I – electric current, [A]	w – average velocity in z -direction, [ms^{-1}]
k – thermal conductivity, [$Wm^{-1}k^{-1}$]	Greek symbols
L – length of duct, [m]	η – overall performance factor
Nu – mean Nusselt number	μ – fluid dynamic viscosity, [$kgm^{-1}m^{-1}$]
Nu_0 – Nusselt number of smooth duct	ρ – fluid density, [kgm^{-3}]
Δp – pressure drop, [Pa]	Acronyms
Q – heat flux, [W]	CR – continuous ribs
Re – Reynolds number	IR – intermittent ribs
s – ribs length, [m]	IRCR – intermittent-continuous-intermittent ribs
T_{in} – inlet temperature, [K]	

References

- [1] Wang, L., Sunden, B., Experimental Investigation of Local Heat Transfer in a Square Duct with Continuous and Truncated Ribs, *Experimental Heat Transfer*, 18 (2005), 3, pp. 179-197
- [2] Han, J. C., Zhang, Y. M., High Performance Heat Transfer Ducts with Parallel Broken and v-Shaped Broken Ribs, *Int. J. Heat Mass Transfer*, 35 (1992), 2, pp. 513-523.1992
- [3] Liou, T. M., Hwang, J. J. Turbulent Heat Transfers Augmentation and Friction in Periodic Fully Developed Channel Flows, *ASME J. Heat Transfer*, 114 (1992), 1, pp. 56-64
- [4] Liou, T. Hwang, J., Effect of Ridge Shapes on Turbulent Heat Transfer and Friction in a Rectangular Channel, *Int. J. Heat Mass Transfer*, 36 (1993), 4, pp. 931-940
- [5] Tanda, G., Heat Transfer in a Rectangular Channel with Transverse and v-Shaped Bribes, *Int. Journal of Heat and Mass Transfer*, 47 (2004), 2, pp. 229-243
- [6] Sahu, M., Bhagoria, J., Augmentation of Heat Transfer Coefficient by Using 90 Broken Transverse Ribs on Absorber Plate of Solar Air Heater, *Renewable Energy*, 30 (2005), 13, pp. 2057-2073
- [7] Wang, L., Sunden, B., Experimental Investigation of Local Heat Transfer in a Square Duct with Various-Shaped Ribs, *Heat and Mass Transfer*, 43 (2007), 8, pp. 759-766, 2007
- [8] Keshmiri, A., et al., Numerical Simulations of Flow and Heat Transfer over Rib-Roughened Surfaces, *International Journal of Heat and Fluid-Flow*, 23 (2002), 6, pp. 750-757
- [9] Rallabandi, A. P., et al., Heat Transfer and Pressure Drop Correlations for Square Channels with 45 Degree Ribs at High Reynolds Number, *Journal of Heat Transfer*, 131 (2009), 071703
- [10] Mushatet, K., et al. Numerical Study of Laminar Flow in a Sudden Expansion Obsteacled Channel, *Thermal Science*, 19 (2015), 2, pp. 657-668
- [11] Skullong, S., Numerical Investigation of Cooling Enhancement with Internal Ribs Coolant Film, *Proceedings*, ASME Turbo Expo, Copenhagen, Denmark, 2012
- [12] Eren, S., et al., Experimental Investigation of Heat Transfer in a Rectangular Channel with Perforated Ribs, *Online Journal of Science and Technology*, 5 (2015), 3, pp. 37-44
- [13] Smaism, G. F., Investigation on Heat Transfer Augmentation Using Continuous and Broken Ribs on a Plate of Heat Exchanger, *International Journal of Energy & Environment*, 9 (2018), 3, pp. 211-232
- [14] Han, J. C., et al., Heat Transfer Enhancement in Channels with Turbulence Promoters, *ASME J. Engineering for Gas Turbines and Power*, 107 (1985), 3, pp. 628-635
- [15] Kumar K. L., *Engineering Fluid Mechanics*, 7th ed., Eurasia Publishing House, New Delhi, India, 1976
- [16] Incopera, F. P., Dewitt, D. P., Introduction Heat Transfer, 4th ed., Wiley, New York, USA, 1985
- [17] Gupta, S., A., et al., Augmented Heat Transfer in Square ducts with Transverse and Inclined Ribs with and without a Gap, *Int. J. Curr. Eng. Technol.*, 3 (2013), 2, pp. 688-694